Inorganic Chemistry

pubs.acs.org/IC

Article

Self-Assembly and Host–Guest Interactions of Pd_3L_2 Metallo-cryptophanes with Photoisomerizable Ligands

Edward Britton, Richard J. Ansell, Mark J. Howard, and Michaele J. Hardie*

Cite This: *Inorg. Chem.* 2021, 60, 12912–12923

Read Online

ACCESS | Metrics & More | Article Recommendations | Supporting Information

ABSTRACT: New photoswitchable pyridyl-azo-phenyl-decorated tripodal host ligands (L_{az}) that belong to the cyclotriveratrylene family have been synthesized, and their photoswitching behavior and crystal structures determined. The latter includes a remarkable 7-fold Borromean-weave entanglement of $\pi-\pi$ stacked layers. Trigonal bipyramidal $\{[Pd(en)]_3(L_{az})_2\}^{6+}$ metallo-cryptophanes (en = ethylenediamine) were formed from these and a previously known pyridyl-azo-phenyl-decorated tripodal host ligand. These coordination cages dissociate at low concentrations and are less robust to photoswitching of the L_{az} ligands than were previously reported Ir(III)-linked metallo-cryptophanes with similar ligands, reflecting the greater lability of the Pd–N bonds. The $\{[Pd(en)]_3(L_{az})_2\}^{6+}$ cages all act as hosts, binding octyl sulfate anions, or *N*-[2-(dimethylamino)ethyl]-1,8-naphthalimide in a dimethyl sulfoxide solution.

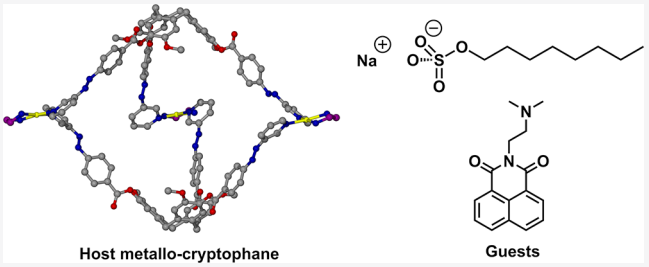

INTRODUCTION

Coordination cages or metallo-cages are three-dimensional assemblies of metal cations and bridging ligands with inherent internal space.[1] Cages may act as host assemblies and bind guest molecules or ions through solvophobic effects and noncovalent interactions. Their binding properties lead to a cornucopia of potential applications in sensor chemistry and catalysis and as nanoscale reaction vessels where confinement of reagents affects properties. The dynamic behavior of coordination cages includes simple ligand exchange and more complex stimulus-responsive behavior, the latter including reconfiguration of cages according to solvent, pH, or other chemical triggers.[2] Coordination cages that are responsive to light form another category of stimulus-responsive cages.[3−11]

Our research focuses on metallo-supramolecular chemistry of the cyclotriveratrylene (CTV) family of host molecules. CTV-type host molecules feature a tribenzo[*a*,*d*,*g*]cyclononene scaffold with a bowl conformation, an open upper rim, and a hydrophobic binding cavity.[12] Tripodal analogues of CTV with ligand groups appended to the upper rim of the bowl are chiral and have proved to be ideal for the self-assembly of metallo-cages, as they have an orthogonal arrangement of metal-binding groups and a deep cavity.[13] The smallest such cages are M_3L_2 metallo-cryptophanes with a trigonal bipyramidal cage shape, noting a cryptophane is an organic cage of two linked CTV fragments. The first examples were $\{[Pd(P\wedge P)]_3L_2\}^{6+}$ metallo-cryptophanes published by Yamaguchi and Shinkai with 4-pyridyl donor groups on the CTV ligand, where P∧P is a chelating phosphine donor ligand.[14] Other $\{[Pd(P\wedge P)]_3L_2\}^{6+}$ examples employ nitrile[15,16] or iso-nicotinoyl[17] donor groups. The use of chelating ligands as coordination-site protecting groups is a common approach to controlling assembly of metallo-cages.[18] Bis-N-heterocyclic carbene chelate ligands have also been successfully employed as protecting ligands for Pd_3L_2 metallo-cryptophanes.[19] Interestingly, a $\{[Pd(en)]_3L_2]^{6+}$ metallocryptophane (en = ethylenediamine) is metastable and undergoes a spontaneous rearrangement in solution to a larger $[Pd_6L_8]^{12+}$ stella octangula cage,[19] behavior also reported for a different class of Pd_3L_2 cages.[20] Other metallo-cryptophanes include luminescent $\{[Ir(C\wedge N)_2]_3L_2\}^{3+}$ cages in which C∧N is a cyclometalling ligand.[10,21] We have recently reported a series of such $\{[Ir(C\wedge N)_2]_3(L_{az})_2\}^{3+}$ cages in which the L_{az} ligands are tripodal CTV analogues functionalized with photo-isomerizable pyridyl-azo-phenyl groups, with an example shown in Figure 1.[10] Each cage contains six pyridyl-azo-phenyl groups that are an inherent part of the cage structure. Azobenzenes (AZB), as well as analogous azoheteroarene species such as these, are some of the most widely used photoswitching motifs and undergo reversible *trans* → *cis* isomerization of the aromatic groups about the azo group.[22] Remarkably, the $\{[Ir(C\wedge N)_2]_3(L_{az})_2\}^{3+}$ cages show reversible photoisomerizations without any change in composition. The

Received: April 28, 2021
Published: August 9, 2021

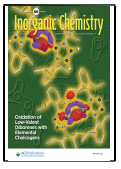

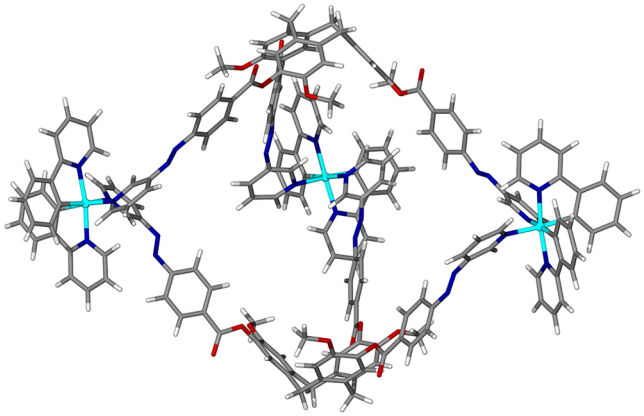

Figure 1. Molecular model of the previously reported $\{[Ir(ppy)_2]_3(L_{az}\text{-}OMe)_2\}^{6+}$ metallo-cryptophane with a CTV-type ligand appended with pyridyl-azo-phenyl groups, all shown in the thermodynamically stable *trans* configuration.[10]

robust nature of the cages to structure switching was in part attributed to the chemical inertness of Ir(III) inhibiting dissociation of the cages.[10]

Examples of coordination cages and two-dimensional polygons that undergo photoisomerization fall into two categories: those in which the photoisomerizable group is pendant to the cage[3] and those in which it is a structurally inherent component of the cage or polygon.[4−8,10,23] Lees et al. have reported photoisomerization of a $[Pd_2Re_2L_4]^{4+}$ metallo-supramolecular square in which L is an azo-bis(4-pyridyl) bridging ligand, which reversibly transforms to a smaller $[PdReL_2]^{2+}$ metallamacrocycle on *trans* → *cis* photoisomerization.[23] Liu and co-workers have reported a $[Pd_2L_4]^{4+}$ cage in which the bridging ligand contains two pyridyl-azo-phenyl groups. This cage completely dissociates upon photoisomerization of the ligand.[4] Clever and co-workers have reported a series of $[Pd_4L_4]^{4+}$ coordination cages that undergo reversible photoisomerization of a structurally inherent bridging ligand while maintaining the integrity of the cage.[5] Here the photoswitching group is a dithienylethene (DTE) in which the structural rearrangement is a ring-open ↔ ring-closed process that is much less dramatic than the *trans* → *cis* rearrangement of AZB. Other examples of cages with DTE-based bridging ligands undergo $[Pd_3L_6]^{6+}$ ↔ $[Pd_{24}L_{48}]^{48+}$ cage transformations on ring-open and ring-closed photoisomerization,[6] and this motif and cage topology switching behavior have been incorporated into soft polymer networks.[7] Wezenberg and Feringa have reported a photoresponsive $[Pd_2L_4]^{4+}$ coordination cage with bridging ligands based on a molecular rotor design of overcrowded alkenes.[8]

We report herein the synthesis of a series of new palladium-linked metallo-cryptophanes, $\{[Pd(en)]_3(L_{az})_2\}^{6+}$, where L_{az} includes the previously reported L_{az}-OMe alongside novel variants with longer-chain ethoxy or propoxy pendant groups on their upper rim (Scheme 1). The presence of propoxy groups rather than methoxy groups on CTV-type ligands affects the solubility of the ligand and has been also shown to affect the relative stabilities of Pd_6L_8 cages.[24] Here, we investigate the influence of the alkyl-chain length on host−guest properties of these metallo-cryptophanes. Palladium(II) is a significantly more labile metal center than is iridium(III).[25] Hence, the photoisomerization behavior of {[Pd-

Scheme 1. Self-Assembly of Metallo-cryptophanes and Numbering Scheme for NMR

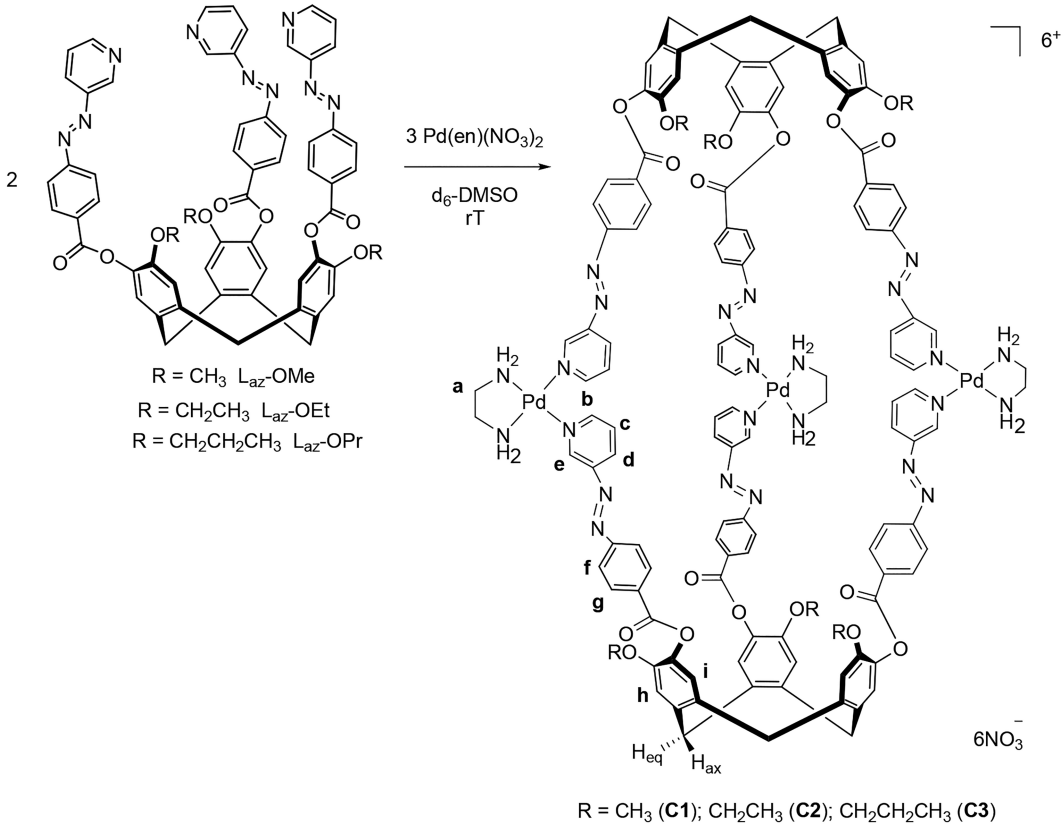

R = CH_3 (**C1**); CH_2CH_3 (**C2**); $CH_2CH_2CH_3$ (**C3**)

https://doi.org/10.1021/acs.inorgchem.1c01297
Inorg. Chem. 2021, 60, 12912−12923

Scheme 2. Synthesis of New Ligands

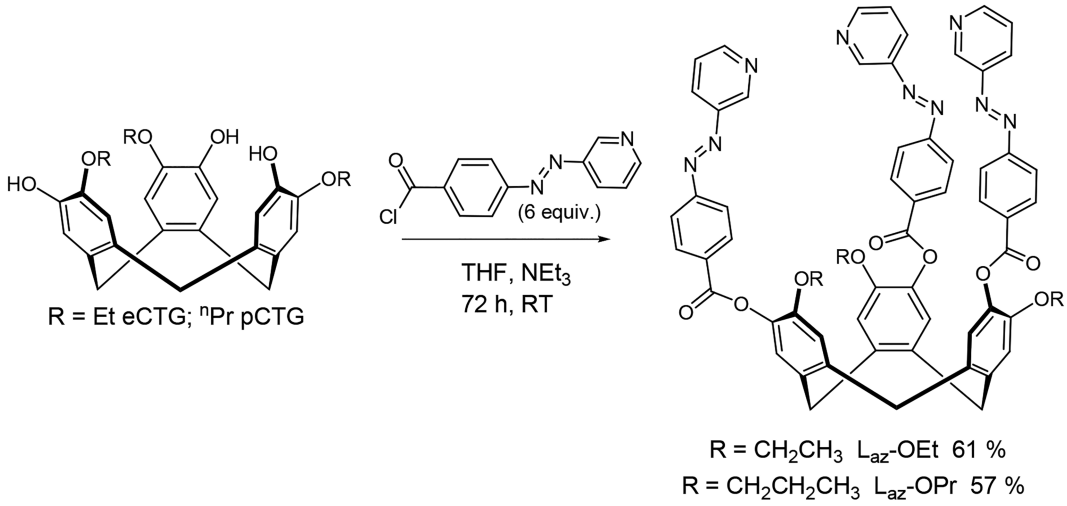

$(en)]_3(L_{az})_2\}^{6+}$ species will allow us to further test whether the kinetic inertness of the metal cage vertices is an important factor in the structural robustness of cages with AZB switches.

RESULTS AND DISCUSSION

Ligand Synthesis and Characterization. The new ligands were synthesized using the same methodology that was used for the previously reported (±)-2,7,12-trimethoxy-3,8,13-tris(3-pyridyl-4-azophenylcarboxy)-10,15-dihydro-5*H*-tribenzo[*a*,*d*,*g*]cyclononene, L_{az}-OMe.[10] Ligands (±)-2,7,12-triethoxy-3,8,13-tris(3-pyridyl-4-azophenylcarboxy)-10,15-dihydro-5*H*-tribenzo[*a*,*d*,*g*]cyclononene (L_{az}-OEt) and (±)-2,7,12-tripropoxy-3,8,13-tris(3-pyridyl-4-azophenylcarboxy)-10,15-dihydro-5*H*-tribenzo[*a*,*d*,*g*]cyclononene (L_{az}-OPr) were synthesized in good yields by reaction of (±)-eCTG [(±)-2,7,12-triethoxy-3,8,13-trimethoxy-10,15-dihydro-5*H*-tribenzo[*a*,*d*,*g*]cyclononatriene][26] and (±)-pCTG [(±)-2,7,12-tripropoxy-3,8,13-trimethoxy-10,15-dihydro-5*H*-tribenzo[*a*,*d*,*g*]cyclononatriene],[24] respectively, with the acid chloride of sodium [2-(3-pyridyl)diazenyl]-benzoate (Scheme 2). Full routes taken to (±)-eCTG and (±)-pCTG are given in the Supporting Information. Ligands were characterized by electrospray mass spectrometry (ESMS), NMR, and ultraviolet−visible (UV−vis) spectroscopies (Supporting Information), all of which are consistent with the proposed structures. An interesting feature of the ESMS spectrum is, alongside the expected *m*/*z* peaks, the appearance of peaks corresponding to dimeric $\{2L + 3H\}^{3+}$ species for both L_{az}-OEt and L_{az}-OPr at *m*/*z* 719.5977 and 747.6284, respectively. This suggests the formation of hydrogen-bonded capsules in the gas phase. Water-mediated hydrogen-bonded capsules of pyridyl-appended CTV analogues have been reported by Purohit and co-workers.[27]

Single crystals of L_{az}-OEt and L_{az}-OPr·$CHCl_3$ were obtained by diffusion of diethyl ether into a saturated solution of each ligand in chloroform. Crystals of both L_{az}-OEt and L_{az}-OPr·$CHCl_3$ were small and required the use of synchrotron radiation to establish their crystal structures. Despite minor differences in chemical composition, the three L_{az} ligands form drastically different crystal structures. The crystal structure of L_{az}-OMe has been previously established and featured columns of bowl-in-bowl L_{az}-OMe host molecules, which interlock through extensive $\pi-\pi$ stacking between the 3-pyridylazophenyl arms to form a network with large open channels with diameters of 25 Å.[10] L_{az}-OEt crystallizes with near-C_3 symmetry with all ethyl groups adopting essentially the same conformation, and all 3-pyridylazophenyl groups are likewise in similar *trans* conformations (Figure 2a). All upper rim groups are co-planar or nearly co-planar with their corresponding arene ring of the cyclononatriene bowl. The L_{az}-OEt hosts stack into homochiral columns in the crystal lattice, adopting an eclipsed bowl-in-bowl stacking separated by an *a* unit cell parameter of 4.7068(3) Å, which is too long to indicate formation of $\pi-\pi$ stacking interactions. The identity of the ligand enantiomer and bowl-up/bowl-down orientation alternate in the crystal lattice in a checkerboard arrangement, and small channels run along the *a* direction (Figure 2b and Figure S55). These are likely occupied by solvent molecules, but the quality of the data obtained did not allow for refinement of solvent positions.

Unlike in L_{az}-OEt, each upper rim arm of L_{az}-OPr in the L_{az}-OPr·$CHCl_3$ complex adopts a different conformation. The $CHCl_3$ is an intracavity guest molecule, forming a C−H···π interaction with one of the arene groups of the cyclononatriene bowl (Figure 3). Each 3-pyridylazophenyl arm of L_{az}-OPr forms a $\pi-\pi$ stacking interaction with its symmetry equivalent around an inversion center with pyridyl ring centroid and pyridyl ring···azo centroid separations of 3.963 and 4.164 Å, 3.855 and 3.659 Å, and 4.190 and 3.626 Å, respectively. This results in the formation of a two-dimensional (2D) hexagonal network of L_{az}-OPr host molecules with 6^3 topology, with alternating ligand enantiomer and bowl-up/bowl-down orientations (Figure 4a). Within a layer of the crystal lattice, there are seven such 2D L_{az}-OPr hexagonal networks. The seven $\pi-\pi$ stacking networks exhibit a remarkable 7-fold 2D → 2D Borromean entanglement (Figure 4). Borromean rings are a type of topological entanglement in which three-ring structures cannot be separated without breaking a ring but there is no catenation or threading between the rings. Synthetic Borromean ring assemblies can be discrete ring assemblies or entangled networks of rings.[28−35] Assemblies with networks of infinite Borromean ring associations fall into two broad categories: infinite chainmail arrays of Borromean associations between discrete rings[29] and Borromean entanglements of 2D networks.[28b,30−34] Borromean entanglement of 2D networks has been reported for coordination poly-

https://doi.org/10.1021/acs.inorgchem.1c01297
Inorg. Chem. 2021, 60, 12912−12923

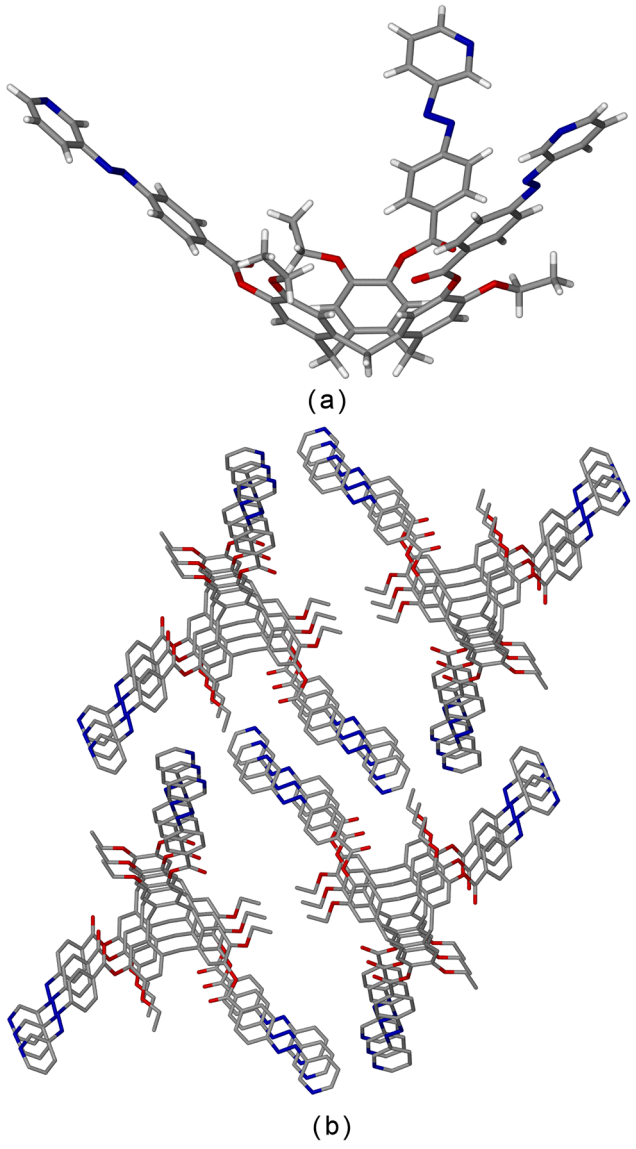

Figure 2. Crystal structure of ligands L_{az}-OEt; (a) asymmetric unit of one ligand and (b) packing diagram showing homochiral stacks. Gray for C, red for O, and blue for N.

mers[28b,30] and hydrogen-bonded,[31,32] halogen-bonded,[33] and argentophilic[34] networks. Borromean entanglement of 2D layers within a self-entangled 3D coordination polymer is also known.[35] A majority of examples involve undulating 2D networks of 6^3 topology as shown here. Known one-dimensional (1D) → 2D and 2D → 2D Borromean entanglements generally show 3-fold entanglement of networks. Examples of 2D → 3D entanglement also feature a traditional Borromean relationship in which each ring within a network is entangled with two others. To the best of our knowledge, however, the 7-fold entanglement observed in L_{az}-OPr·$CHCl_3$ is only the second example of such a higher-order Borromean entanglement of networks. The first was also a 7-fold Borromean entanglement of a 2D 6^3 network, in this case a hydrogen-bonded network.[32] Borromean chainmail structure is also of higher order and features discrete but interlocked M_6L_6 metallamacrocyles that also involved a tripodal CTG derivative as the ligand.[29]

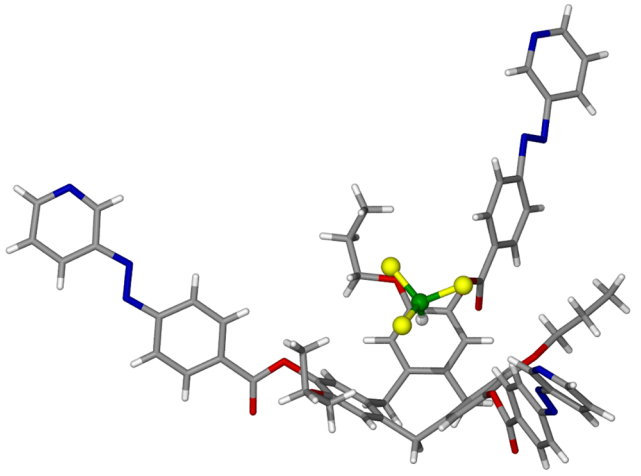

Figure 3. Asymmetric unit of the crystal structure of L_{az}-OPr·$CHCl_3$ highlighting host–guest interactions. $CHCl_3$ shown with C colored green. Otherwise gray for C, red for O, blue for N, yellow for Cl, and white for H.

The UV–vis spectra of ligands L_{az}-OMe, L_{az}-OEt, and L_{az}-OPr in $CHCl_3$ are similar, each showing a strong π–π^* absorption band near 325 nm and a weak n–π^* band at 450 nm. A *trans* → *cis* photoisomerization of azobenzene moieties leads to a decrease in the intensity of the π–π^* band and a concomitant marginal increase in the intensity of the n–π^* band. Irradiation of the 30 μM chloroform solutions of each ligand with a 30 W 365 nm lamp for a total of 60 s led to very similar spectral changes indicative of photoisomerization, shown for L_{az}-OEt in Figure 5 (see the Supporting Information for other ligands). Irradiation beyond 60 s did not lead to further spectral changes. Under these conditions, 52–54% of the *trans* 3-pyridylazophenyl groups of each ligand were converted to the *cis* isomer. The presence of three 3-pyridylazophenyl arms per ligand means that there are four possible isomers on photoswitching: *trans*–*trans*–*trans*, *trans*–*trans*–*cis*, *trans*–*cis*–*cis*, and *cis*–*cis*–*cis*. The photoswitched ligand solutions are likely to contain a mixture of these isomers. Indeed, previous ^{1}H NMR studies of the photoswitching behavior of L_{az}-OMe indicate that this is the case.[10]

$\{[Pd(en)]_3(L_{az})_2\}^{6+}$ Metallo-cryptophanes. Metallo-cryptophane cages of the $\{[Pd(en)]_3(L_{az})_2\}^{6+}$ type can be assembled for L_{az}-OMe (**C1**), L_{az}-OEt (**C2**), and L_{az}-OPr (**C3**) by self-assembly of a 3:2 mixture of $[Pd(en)(NO_3)_2]$ and the appropriate L_{az} ligand in dimethyl sulfoxide (DMSO) (Scheme 1). The use of other solvents such as acetonitrile or nitromethane did not result in cage formation. All three cages showed similar NMR spectra. All resonances of their ^{1}H NMR spectra were broadened slightly and remained relatively straightforward, consistent with the formation of a symmetric larger species such as metallo-cryptophane, shown for complex **C1** in Figure 6 (see the Supporting Information for other complexes). In each complex, signals for the two protons situated *ortho* to the pyridyl nitrogen exhibited a downfield shift from ~9.2 to 9.6 ppm (H_e) and from ~8.75 to 9.15 ppm (H_b), consistent with binding of the pyridyl nitrogen to the palladium center. Cages **C1** and **C2** were further characterized by $^{13}C\{^1H\}$ NMR, which reveals a consistent number of peaks with the proposed structure, and 2D NMR techniques COSY, HSQC, and HMBC, allowing for the complete assignment of all proton environments (Figures S15–S18 and S23–S26).

https://doi.org/10.1021/acs.inorgchem.1c01297
Inorg. Chem. 2021, 60, 12912–12923

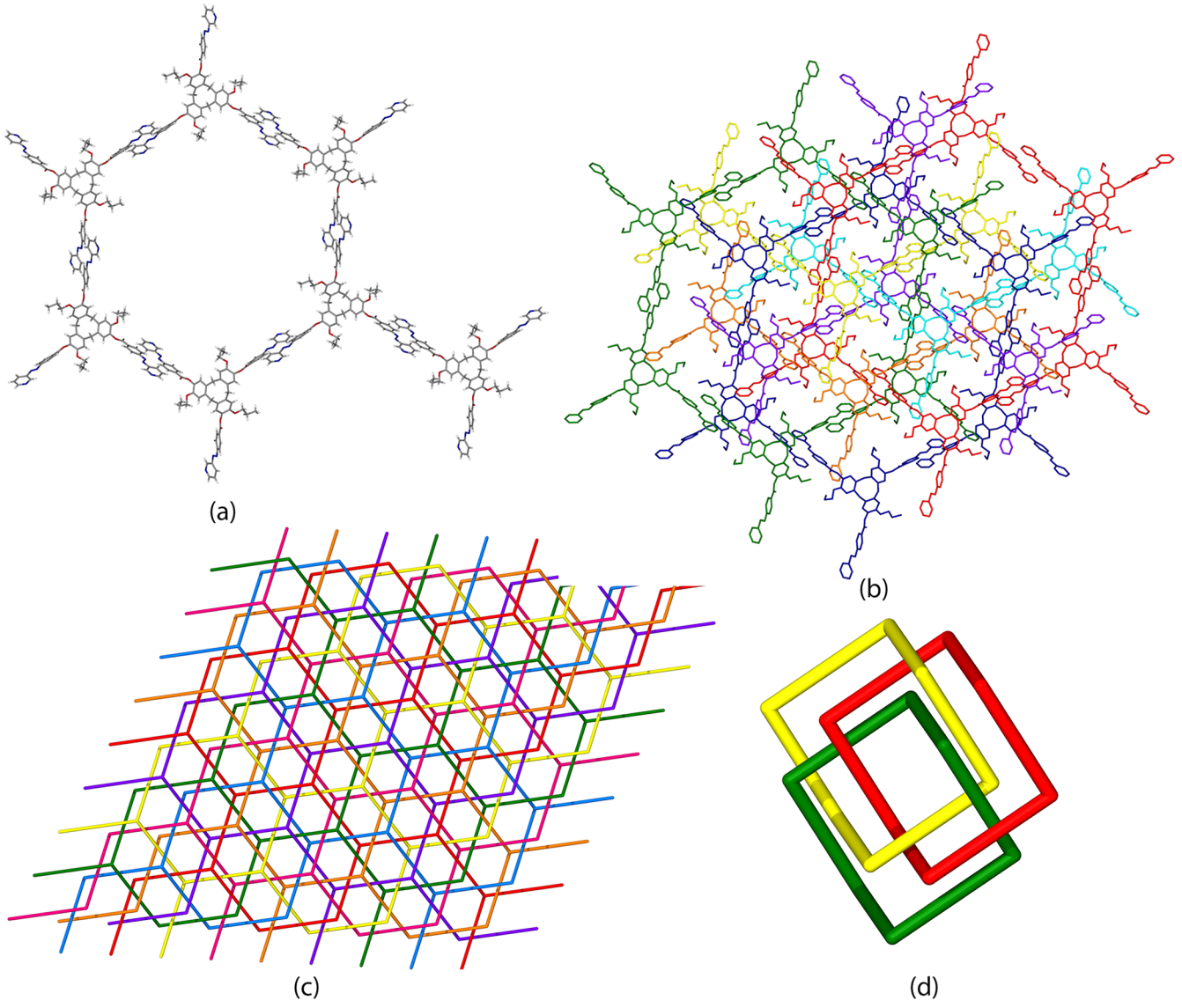

Figure 4. From the crystal structure of L_{az}-OPr·$CHCl_3$. (a) $\pi-\pi$ stacking interactions forming a 2D network of 6^3 topology. (b) Detail showing seven entangled $\pi-\pi$ stacking networks within a layer. (c) Connectivity diagram highlighting the 7-fold Borromean entanglement of networks with a single Borromean ring association between these network highlighted in panel d.

The $^1H-^1H$ NOESY NMR spectrum obtained for **C2** (Figure 6b) displays the expected cross-coupling between the amine protons on the palladium ethylenediamine complex and the *ortho* pyridyl protons on the ligand ($H_{e/b}$), which would be in the proximity in the proposed structure. Similar cross-couplings were seen in $^1H-^1H$ NOESY spectra of samples of each of the cages obtained during host–guest studies (Figures S43–S45). ^1H DOSY NMR spectra of each of **C1–C3** were also consistent with cage formation (Figures S19, S27, and S30). ESMS run under standard dilution conditions did not show cages in solution due to cage dissociation at low concentrations, with the spectra dominated by free ligands (Figures S32 and S33). We could obtain an ESMS spectrum for a concentrated solution of **C1** that gave the expected 6+ peak at m/z 428.1710 (calculated m/z 428.4311 for $\{[Pd(en)]_3(L_{az}\text{-}OMe)_2\}^{6+}$) (Figure S31).

Closer analysis of the ^1H NMR spectra of **C1–C3** revealed that, alongside the major peaks that can be attributed to the metallo-cryptophane, there were a number of much smaller signals that align perfectly with the free ligands, albeit somewhat broadened (Figures 6a and Figures S22 and S29). This may indicate exchange between the free ligand and the metallo-cryptophane. There were no peaks in the spectra that could be attributed to any intermediate species such as $[M_2L_2]^{4+}$. This implies that while the cryptophane species may be in rapid exchange with its constituent parts, the process of metallo-cryptophane formation becomes progressively more energetically favorable once formation has started with an $[ML]^+$ species. This behavior has been observed for self-assembled systems previously, for example, Lehn's helicates.[36] The ^1H NMR spectra of **C1–C3** did not sharpen, or change appreciably, on standing for several months. The latter is notable, as our previous studies of $\{[Pd(en)]_3(L_{py})_2\}^{6+}$ cages in which L_{py} is an isonicotinoyl-appended CTG ligand revealed a rearrangement to a larger stella octangula Pd_6L_8 cage on standing in solution for 2 weeks.[24] Furthermore, $\{[Ir(C\wedge N)_2]_3(L_{py})_2\}^{3+}$ cages exhibit spectral sharpening associated

https://doi.org/10.1021/acs.inorgchem.1c01297
Inorg. Chem. 2021, 60, 12912–12923

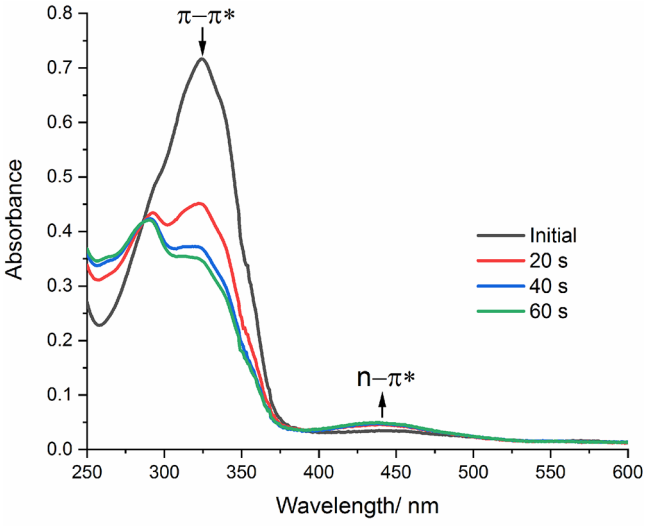

Figure 5. UV−vis spectrum of L_{az}-OEt (30 μM, $CHCl_3$) upon irradiation with 365 nm light. The decreasing intensity of the $\pi-\pi^*$ band at 325 nm and the increasing intensity of the n−π^* band at ∼440 nm are indicative of *trans* → *cis* isomerization.

with chiral self-sorting of L_{py} ligands over a 3 month equilibration period.[21]

The photoswitching behavior of **C1** was studied as an exemplar for these cages. Photoswitching of **C1** in a DMSO solution was monitored by ^{1}H NMR and ion-mobility mass spectrometry (IM-MS). UV−vis spectroscopy is typically used to monitor photoswitching but requires high dilution. Dilution of a solution of **C1** to 30 μM, which is a typical concentration for UV−vis spectroscopy, resulted in complete disassembly of the metallo-cryptophane cage (Figure S20). Pd(II)-pyridyl bonds are relatively labile, and this reversibility means that at very low concentrations of the cage the backward reactions can dominate due to Le Chatelier's principle. This behavior is consistent with previous reports of a nitrile-appended palladium metallo-cryptophane in dichloromethane that begins to disassemble at concentrations below approximately 200 μM when monitored by ^{1}H NMR.[16]

A 600 μM solution of **C1** was irradiated with a 355 nm Nd:YAG laser[37] for a total exposure of 1200 s, and a ^{1}H NMR spectrum acquired. The NMR spectrum of the irradiated sample is considerably broadened, as was seen for $\{[Ir(C\wedge N)_2]_3(L_{az}\text{-OMe})_2\}^{3+}$,[10] which is anticipated if a mixture of *cis* and *trans* isomers is present (Figure S21). However, a new, sharp peak appears in the spectrum at ∼4.8 ppm, which was not anticipated. Furthermore, if the solution is switched back to *trans*-L_{az}-OMe by exposure to 450 nm light, the ^{1}H NMR spectrum of the resultant sample is clearly a mixture of free L1-OMe and metallo-cryptophane **C1**, alongside the peak at 4.81 ppm, assigned as a $[Pd(en)_2]^{2+}$ species (Figure S21). Irradiation of **C1** for accumulation times of >1200 s resulted in the formation of palladium black. Thus, unlike the $\{[Ir(C\wedge N)_2]_3(L_{az})_2\}^{3+}$ cages, $\{[Pd(en)]_3(L_{az}\text{-OMe})_2\}^{6+}$ is less robust and undergoes partial disassembly on photoisomerization of 3-pyridylazophenyl groups.

IM-MS measures the time taken for a species to diffuse along a drift tube against the flow of a carrier gas and has recently found application in supramolecular chemistry.[38] Species with a larger radius of diffusion take longer to flow across the tube; hence, any significant change in size of an intact $\{[Pd(en)]_3(L_{az}\text{-OMe})_2\}^{6+}$ cage upon photoirradiation should be observable as a change in drift time with anticipated broadening of the distribution curve. This was not observed, and peaks corresponding to the $\{[Pd(en)]_3(L_{az}\text{-OMe})_2\}^{6+}$ cage were very similar for the parent and irradiated solutions (Figures S34 and S35). Thus, there is no evidence of the presence of a $\{[Pd(en)]_3(L_{az}\text{-OMe})_2\}^{6+}$ cage with any L_{az}-OMe ligands in the *cis*, or partial *cis*, configuration, and the observed metallo-cryptophane is an unswitched all-*trans* cage.

Host−Guest Studies. A range of other neutral and anionic molecules were screened for host−guest interactions with the metallo-cryptophanes, including fullerenes, borane salt $Cs_2B_{12}F_{12}$, sodium octyl sulfate, haloalkanes, and a naphthalamide derivative. Fullerenes, in particular, are widely documented to form host−guest association with CTV and many of its analogues or derivatives.[39] Of the potential guests tried, only sodium octyl sulfate [SOS (Chart 1)] and naphthalimide derivative *N*-[2-(dimethylamino)ethyl]-1,8-naphthalimide [**nap** (Chart 1)] exhibited any evidence of forming host−guest interactions with the metallo-cryptophanes.

We have previously reported the 1:2 host:guest (H:G) binding of alkyl sulfate surfactant anions by the $[Pd_6(L_{py})_8]^{12+}$ stella octangula cage.[40] Jung and co-workers have recently reported a distinct Pd_6L_8 cage that binds a range of alkyl sulfate surfactants in which the cage shows a breathing-type flexibility induced by guest binding.[41] Surfactant anions have an anionic headgroup capable of electrostatic interactions with the palladium centers, and a hydrophobic tail capable of C−H···π interactions with the walls of the cage. The binding behavior of **C1**−**C3** in a DMSO solution to SOS was investigated via binding experiments that were performed with guest concentrations ranging from 1.0 to 40 mM. While this is below the critical micelle concentration for SOS,[42,43] self-titration experiments with SOS in DMSO monitored by ^{1}H NMR did show minor chemical shift changes indicative of some aggregation at these concentrations (Figure S36).

Titration of a solution of SOS into a 3.85 mM solution of each of the metallo-cryptophane cages **C1**−**C3** resulted in distinct ^{1}H NMR chemical shift changes for all proton environments of the SOS along with some proton environments of the cages. There was only one set of signals for the SOS guest indicating those bound and unbound guests are likely to be exchanging faster than the NMR time scale. The plot of chemical shift changes versus SOS concentration for the SOS methyl proton (H_m) for all three cages is shown in Figure 7, and similar binding isotherms were observed by monitoring chemical shift changes for methylene SOS protons (H_l) and pyridyl-H_e of the L_{az} ligands within each cage. The chemical shift change data were fit using HypNMR2008.[44] A range of binding stoichiometries were tested, including 1:1, 1:2, and 1:3 H:G ratios, both with and without a guest self-association factor (G2). The best fit-to-data model was found for a 1:1 H:G ratio with a dimeric G2 guest association also factored in. Predicted chemical shift changes for all monitored protons ($H_{j/k/m}$ of the guest and H_e of the host) were an excellent match to data for all three metal-cryptophanes (Figures S40−S42). A 1:1 H:G model without consideration of guest self-association gave a poor fit to data for the chemical shift of the SOS−OCH_2-R proton (Figure S40b). This is notably the proton environment that displayed chemical shift changes during the self-titration experiments with SOS. The 1:1 binding constants are listed in Table 1. The binding of the

https://doi.org/10.1021/acs.inorgchem.1c01297
Inorg. Chem. 2021, 60, 12912−12923

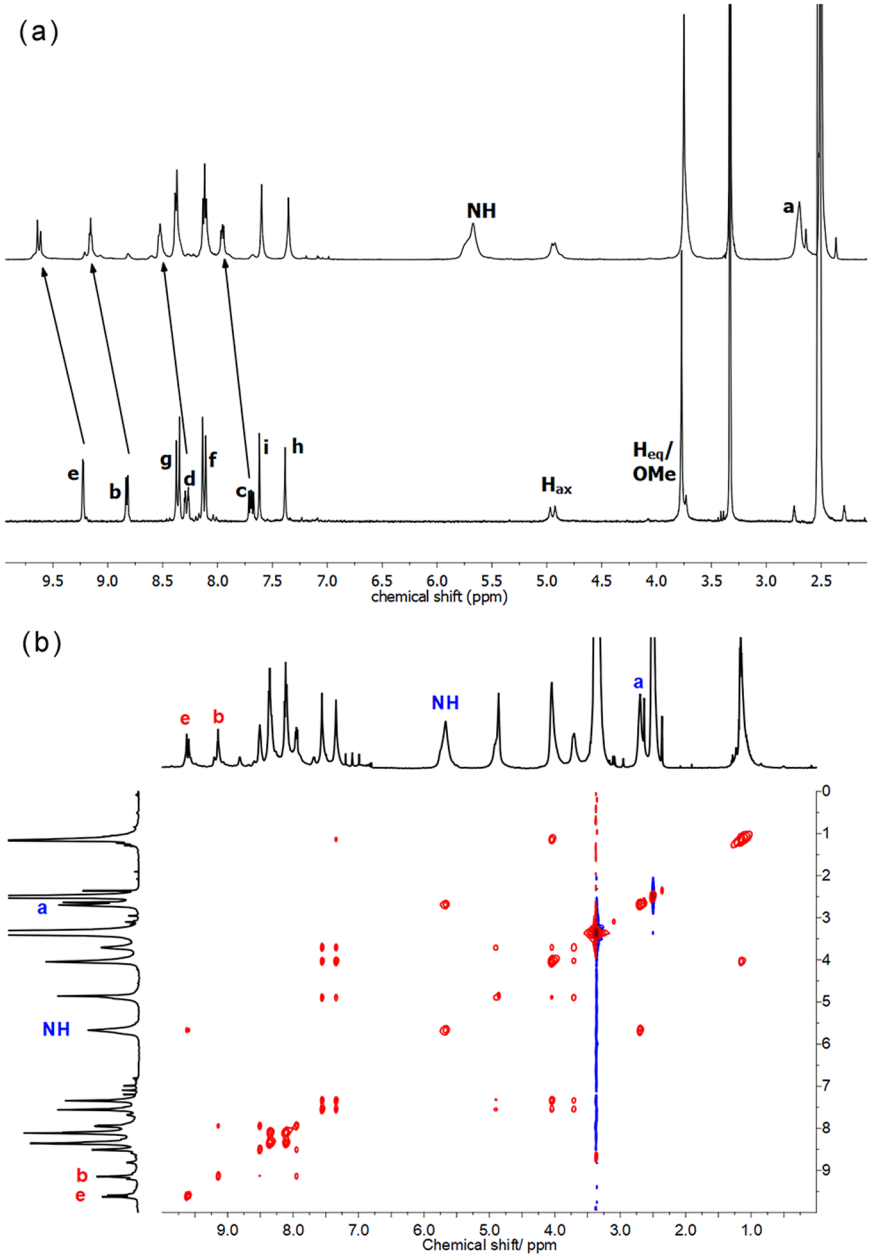

Figure 6. ^{1}H NMR spectra of metallocryptophanes in d_6-DMSO. (a) 1D spectra of ligand L_{az}-OMe (bottom) and **C1** (top). (b) ^{1}H−^{1}H NOESY spectrum of **C2**.

Chart 1. Guest Species Bound by Cages

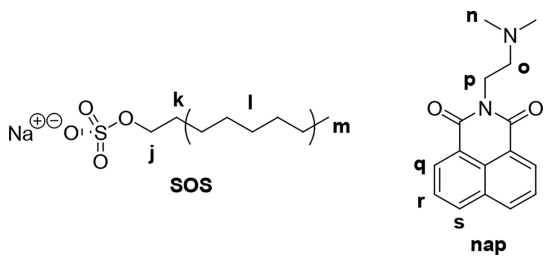

sodium alkyl sulfates by cages **C1**−**C3** is considerably weaker than for similar systems. There is no obvious correlation between alkoxide-chain length on the L_{az} ligand of the cage and the binding constant. The lowest binding constant was, however, found for the cage with L_{az}-OMe, where guest access into and out of the metallo-cryptophane windows is least impeded by the side arm chain. The larger $[Pd_6(L_{py})_8]^{12+}$ stella octangula cage bound SOS with a K_a of 1×10^6 M^{-1} for 1:2 H:G binding.[40] A 1:1 H:G complex between SOS and a curcubit[7]uril-based receptor was reported by Yu and co-workers with a K_a of 2.4×10^4 M^{-1}.[45]

^{1}H−^{1}H NOESY NMR spectra were acquired to further probe the nature of the host−guest interaction. Through-space couplings were observed for only the [SOS]@**C3** system, possibly as the longer propoxy groups on the **C3** cage hinder guest exchange rates more than would the cages with the shorter alkoxy groups. Another explanation is that the propoxy groups themselves occupy space with the metallo-cryptophane cage, inhibiting guest dynamics within the cage. Given the 1:1

https://doi.org/10.1021/acs.inorgchem.1c01297
Inorg. Chem. 2021, 60, 12912−12923

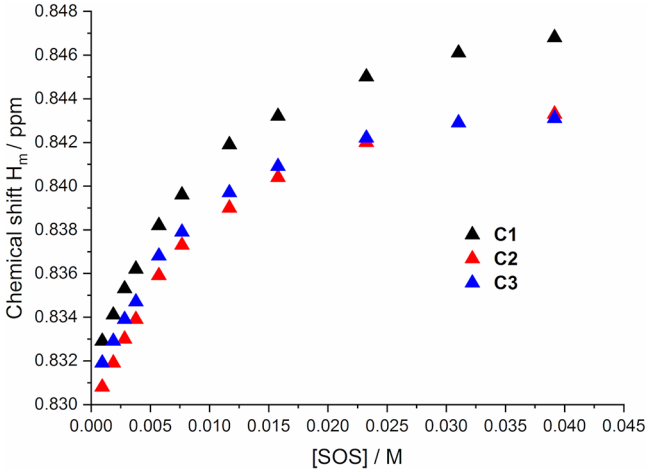

Figure 7. Binding isotherms showing ^{1}H NMR chemical shift changes in d_6-DMSO for SOS methyl proton H_m upon titration into a 3.85 mM solution of metallo-cryptophanes.

Table 1. Binding Constants Obtained for SOS Binding by Cages C1−C3

	C1	C2	C3
K_{aG2} (M^{-1})	16.2 ± 1.6	5.1 ± 3.3	9.1 ± 5.5
K_{aHG} (M^{-1})	68.6 ± 1.9	299.0 ± 9.2	115.9 ± 6.9

H:G binding ratio gives a guest occupancy somewhat below the 55% guest-to-void volume ratio established as ideal by Rebek and co-workers,[46] the latter explanation may be the most pertinent. Through-space couplings were observed between the methylene protons on SOS, H_l, and the phenyl ring of the azo group found on the host architecture, H_f and H_g (Figure 8), consistent with in-cage binding of the octyl sulfonate anion and pointing to the formation of CH−π interactions between the guest and host.

Self-titration of **nap** in d_6-DMSO showed small chemical shift changes, most notably upfield shifts for the protons on the naphthalene group, likely due to $\pi-\pi$ stacking interactions.[47] Guest **nap** was titrated into 2.75 mM solutions of cages **C1**−**C3** in d_6-DMSO, over a guest concentration range of 0.28−27.5 mM. In all cases, clear chemical shift changes were observed for **nap**, which were different from those seen in self-titration experiments with **nap**. The free guest and bound guest are in exchange, and the **nap**−$CH_2C\underline{H}_2NMe_2$ (H_o) proton was used to monitor the binding as it showed the largest chemical shift change without being obscured by peaks from cage or solvent proton environments. Binding isotherms are shown in Figure 9. The behavior was not the same for all three cages,

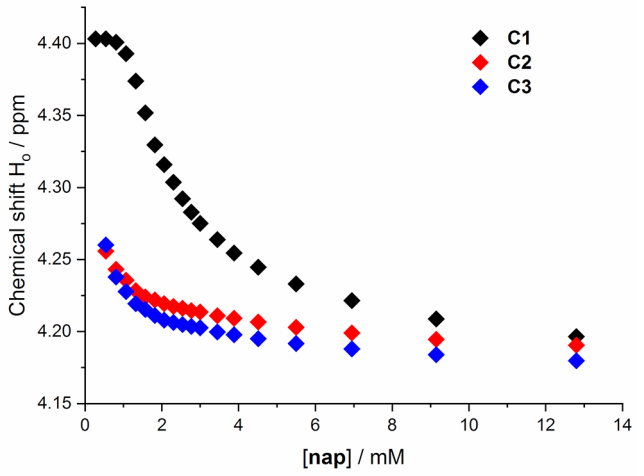

Figure 9. Binding isotherms showing ^{1}H NMR chemical shift changes in d_6-DMSO for **nap** proton H_o upon titration into a 2.75 mM solution of metallo-cryptophanes **C1**−**C3**.

with cage **C1** inducing the greatest chemical shift change. Furthermore, where the metallo-cryptophane **C1** is the host, the system is in fast exchange on the NMR time scale, evidenced by the appearance of the **nap**−$CH_2C\underline{H}_2NMe_2$ proton (H_o) as a clear triplet in the high- and low-

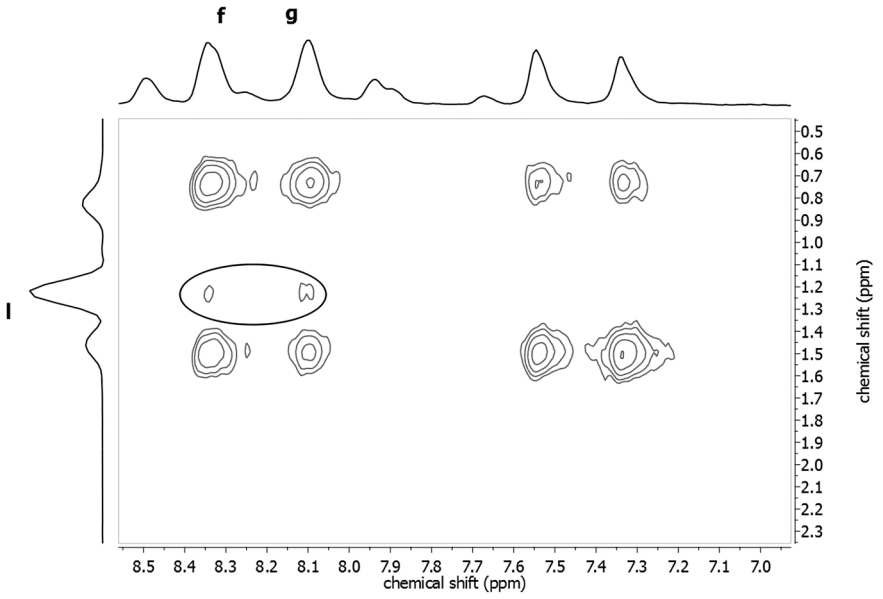

Figure 8. ^{1}H−^{1}H NOESY spectrum (500 MHz, d_6-DMSO) of **C3** and SOS. Circled peaks indicate through-space interactions between guest methylene protons H_l and host arene protons H_f and H_g.

https://doi.org/10.1021/acs.inorgchem.1c01297
Inorg. Chem. 2021, 60, 12912−12923

concentration regimes with only a slight broadening at intermediate concentrations.[48] Whereas when **C2** or **C3** is the metallo-cryptophane host, the system is exchanging at a slower rate, approximately in the intermediate exchange region on the NMR time scale. For these cases, the **nap** H_o proton is observed as only a triplet at high concentrations of **nap**, where it exists mostly unbound in solution. At lower concentrations, the signal broadens until at very low concentrations, when nearly all of **nap** will be in exchange, the signal broadens to such a degree it becomes indistinguishable from the baseline (Figure S50). Hence, the longer ethoxy and propoxy side arms of the L ligands of **C2** and **C3**, respectively, sterically hinder access to the internal space of the cage, resulting in a larger kinetic barrier to encapsulation and de-encapsulation, slowing the process, which has the effect of broadening the NMR signals.[48] The effect of the size of portals between the exterior and interior of a cage and the kinetics of host−guest system is well-documented.[49] Attempts to fit the binding isotherms in Figure 9 to 1:1, 1:2, and 1:3 H:G models were not successful. As additional evidence for binding, the **nap@C1** and **nap@C2** systems were further investigated by ^{1}H DOSY NMR. Despite their significant difference in size, the diffusion constants for **nap** and the cages were very similar, indicative of host−guest binding (Figure S51). The DOSY experiment also confirms that the metallo-cryptophane cage remains intact in the presence of **nap**.

CONCLUSIONS

Tripodal cavitand ligands based on a tribenzo[*a,d,g*]-cyclononene scaffold with appended 3-pyridyl-azo-phenyl groups can self-assemble with a *cis*-protected Pd(II) species to form trigonal bipyramidal $\{[Pd(en)]_3(L_{az})_2\}^{6+}$ cages of the metallo-cryptophane family but disassemble at low concentrations. Unlike some previously reported metallo-cryptophanes, ethylenediamine is a suitable *cis*-protecting chelate ligand for these cages and M_3L_2 to M_6L_8 cage rearrangement does not occur. The ligands themselves all exhibit the reversible *trans* → *cis* photoisomerization that is typical of azoheteroarene species. However, there is no evidence that the $\{[Pd(en)]_3(L_{az})_2\}^{6+}$ cages can be photoisomerized while maintaining their cagelike structure. A solution of $\{[Pd(en)]_3(L_{az}\text{-}OMe_2)\}^{6+}$ shows spectral changes upon exposure to first 355 nm light and then 450 nm light but is accompanied by clear evidence of a significant degree of dissociation of the cage. This behavior is in direct contrast to that of the previously studied $\{[Ir(C\wedge N)_2]_3(L_{az}\text{-}OMe)_2\}^{3+}$ cages, where spectral data indicated reversible photoswitching and no compositional change to the cage in its *cis*-rich form. The higher level of robustness of the Ir(III) cages compared with the Pd(II) cages is likely to be a consequence of the higher degree of lability of Pd(II). This suggests that the use of inert metals, while significantly slowing self-assembly processes, is a useful tool for the synthesis of shape-changing metallocages.

All three $\{[Pd(en)]_3(L_{az})_2\}^{6+}$ metallo-cryptophanes behaved as nanoscale host assemblies in DMSO solutions and were shown to bind disparate guests, namely, an anionic surfactant, sodium octyl sulfate, and naphthalimide derivative *N*-[2-(dimethylamino)ethyl]-1,8-naphthalimide. Subtle differences in the binding behavior of the three cage hosts may be due to a degree of self-binding in which the longer alkyl chains of L_{az}-OPr in particular are able to restrict guest access to the cage portals or themselves occupy space within the hydrophobic cage interior.

EXPERIMENTAL SECTION

Synthesis. ^{1}H and ^{13}C NMR spectra (including COSY, HSQC, HMBC, and NOESY spectra) were recorded using a Bruker AV-NEO 11.4 T instrument (500 MHz ^{1}H) with a 5 mm DCH cryoprobe or 5 mm TBO RT-probe and a Bruker 400 MHz NMR spectrometer with a 5 mm BBFO RT-probe. Diffusion ordered spectroscopy (DOSY) measurements were taken using a Jeol ECA 14.1 T (600 MHz ^{1}H) spectrometer with a 5 mm ROYAL probe. The pulse sequences used a bipolar pulse pair simulated echo (BPPSTE). High-resolution electrospray mass spectra (ESI-MS) were recorded on a Bruker micro-TOF-Q mass spectrometer. IM-MS was performed on a Synapt G2-Si Imaging Mass Spectrometer.

(±)-2,7,12-Tripropoxy-3,8,13-trimethoxy-10,15-dihydro-5*H*-tribenzo[*a,d,g*]cyclononatriene (pCTG),[22] 3-(4-benzoyl chlorideazo)-pyridine,[10] and (±)-2,7,12-trimethoxy-3,8,13-tris(3-pyridyl-4-azophenylcarboxy)-10,15-dihydro-5*H*-tribenzo[*a,d,g*]cyclononatriene (L_{az}-OMe)[10] were synthesized according to previously published procedures. A new route to 2,7,12-triethoxy-3,8,13-trimethoxy-10,15-dihydro-5*H*-tribenzo[*a,d,g*]cyclononatriene (eCTG)[26] was employed via (±)-2,7,12-triethoxy-3,8,13-tris(propenyloxy)-10,15-dihydro-5*H*-tribenzo[*a,d,g*]cyclononatriene, the latter synthesized by literature procedures.[50] Detailed ^{13}C{^{1}H} NMR assignments of L_{az}-OEt and L_{az}-OPr are given in the Supporting Information.

(±)-2,7,12-Triethoxy-3,8,13-trihydroxy-10,15-dihydro-5H-tribenzo[a,d,g]cyclononatriene (eCTG). (±)-2,7,12-Triethoxy-3,8,13-tris(propenyloxy)-10,15-dihydro-5*H*-tribenzo[*a,d,g*]-cyclononatriene (1.90 g, 3.36 mmol) and triphenylphosphine (0.26 g, 1.01 mmol) were dissolved in a mixture of diethylamine (15 mL), water (15 mL), and anhydrous THF (80 mL) under an atmosphere of N_2. The solution was heated to reflux, and palladium(II) acetate (0.04 g, 0.17 mmol) was added in one portion. The solution was heated overnight, and the resultant black suspension was filtered through Celite to yield an orange solution. The solvent was removed, and the residue was triturated in ethanol. The product was filtered and washed with ethanol and then diethyl ether to yield the product as an off-white powder (1.03 g, 2.29 mmol, 68%). ^{1}H NMR (300 MHz, $CDCl_3$): δ 6.86 (s, 3H, ArH), 6.78 (s, 3H, ArH), 5.44 (bs, 3H, OH), 4.69 (d, 3H, J = 13.7 Hz, $-CH_{ax}H-$), 4.08 (q, 6H, J = 7.0 Hz, $-OCH_2CH_3$), 3.47 (d, 3H, J = 13.8 Hz, $-CH_{eq}H-$), 1.40 (t, 9H, J = 7.0 Hz, $-OCH_2CH_3$). ^{13}C{^{1}H} NMR (75 MHz, $CDCl_3$): δ 143.5, 143.2, 131.4, 130.2, 114.3, 112.2, 63.6, 35.2, 13.8. ESI-MS (+ve) $[M + Na]^+$: m/z 473.1936, calcd m/z 473.1940. Data consistent with the literature.[26]

(±)-2,7,12-Triethoxy-3,8,13-tris(3-pyridyl-4-azophenylcarboxy)-10,15-dihydro-5H-tribenzo[a,d,g]cyclononatriene (L_{az}-OEt). eCTG (219 mg, 0.49 mmol) was dissolved in anhydrous THF (60 mL) under N_2; anhydrous triethylamine (6 mL) was added, and the mixture was stirred for 30 min. The solution was transferred to a flask containing 3-(4-benzoyl chlorideazo)pyridine (738 mg, 2.96 mmol) and stirred at room temperature for 3 days. The suspension was filtered, and the eluent was collected. The solvent was removed to yield an orange residue that was triturated in methanol (200 mL), filtered, and washed with methanol and diethyl ether to yield the product as a bright orange powder (323 mg, 0.30 mmol, 61%). ^{1}H NMR (500 MHz, $CDCl_3$): δ 9.25 (s, 3H, H_e), 8.75 (d, 3H, J = 4.4 Hz, H_b), 8.36 (d, 6H, J = 6.8 Hz, H_g), 8.18 (d, 3H, J = 8.0 Hz, H_d), 8.04 (d, 6H, J = 8.0 Hz, H_f), 7.47 (m, 3H, H_c), 7.20 (s, 3H, H_i), 6.99 (s, 3H, H_h), 4.83 (d, 3H, J = 13.6 Hz, $-CH_{ax}H-$), 4.07 (q, 6H, J = 6.8 Hz, $-OCH_2CH_3$), 3.68 (d, 3H, J = 13.6 Hz, $-CH_{eq}H-$), 1.26 (t, 9H, J = 6.8 Hz, $-OCH_2CH_3$). ^{13}C{^{1}H} NMR (125 MHz, $CDCl_3$): δ 164.2, 155.2, 152.5, 149.3, 147.9, 147.8, 139.2, 138.2, 132.1, 131.8, 131.5, 127.2, 124.2, 124.1, 123.1, 115.8, 65.0, 36.7, 14.9. ESI-MS (+ve) $[M + H]^+$: m/z 1078.3662, calcd m/z 1078.3883.

(±)-2,7,12-Tripropoxy-3,8,13-tris(3-pyridyl-4-azophenylcarboxy)-10,15-dihydro-5H-tribenzo[a,d,g]cyclononatriene (Laz-OPr). pCTG (118 mg, 0.24 mmol) was dissolved in anhydrous THF (30 mL) under N_2; anhydrous triethylamine (3 mL) was added, and the mixture was stirred for 30 min. The solution was transferred to a flask containing 3-(4-benzoyl chlorideazo)pyridine (363 mg, 1.48 mmol) and stirred at room temperature for 3 days. The suspension was

https://doi.org/10.1021/acs.inorgchem.1c01297
Inorg. Chem. 2021, 60, 12912−12923

filtered, and the eluent was collected. The solvent was removed to yield an orange residue that was triturated in methanol (100 mL), filtered, and washed with methanol and diethyl ether to yield the product as a bright orange powder (154 mg, 0.14 mmol, 57%). ^{1}H NMR (500 MHz, $CDCl_3$): δ 9.25 (s, 3H, H_e), 8.75 (d, 3H, J = 1.5, 4.8 Hz, H_b), 8.36 (d, 6H, J = 9.0 Hz, H_g), 8.19 (dt, 3H, J = 1.5, 8.1 Hz, H_d), 8.04 (d, 6H, J = 8.7 Hz, H_f), 7.48 (dd, 3H, J = 4.8, 8.1 Hz, H_c), 7.21 (s, 3H, H_i), 6.98 (s, 3H, H_h), 4.85 (d, 3H, J = 15.0 Hz, $-CH_{ax}H-$), 3.97 (m, 6H, -$OCH_2CH_2CH_3$), 3.69 (d, 3H, J = 13.8 Hz, $-CH_{eq}H-$), 1.68 (sextet, 6H, J = 7.2 Hz, -$OCH_2CH_2CH_3$), 0.88 (t, 9H, J = 7.2 Hz, -$OCH_2CH_2CH_3$). ^{13}C NMR (126 MHz, $CDCl_3$): δ 164.2, 155.2, 152.6, 149.4, 147.9, 147.7, 139.1, 138.2, 132.1, 131.6, 131.5, 127.1, 124.2, 124.0, 123.1, 115.6, 70.7, 36.7, 22.6, 10.5. ESI-MS (+ve) $[M + H]^+$: m/z 1120.4137, calcd m/z 1120.4352.

General Procedure for Cage Assembly. The appropriate L_{az} (4.0 mg) was dissolved in d_6-DMSO (0.3 mL). $Pd(en)(NO_3)_2$ (1.5 equiv) was dissolved in d_6-DMSO (0.3 mL) and added dropwise to the solution of L_{az}. The bright orange solution was left to stand for 5 min after which time a ^{1}H NMR spectrum was acquired.

{[Pd(en)]$_3$(L_{az}-OMe)$_2$}·6(NO_3) ***(C1)***. ^{1}H NMR (500 MHz, d_6-DMSO): δ 9.62 (d, 6H, J = 13.3 Hz, H_e), 9.15 (bs, 6H, H_b), 8.52 (bs, 6H, H_d), 8.37 (d, 12H, J = 8.5 Hz, H_g), 8.11 (t, 12H, J = 8.3 Hz, H_f), 7.95 (t, 6H, J = 8.1 Hz, H_c), 7.60 (s, 6H, H_i), 7.35 (s, 6H, H_h), 5.67 (bs, 15H, NH), 4.93 (d, 6H, J = 14.1 Hz, $-CH_{ax}H-$), 3.75 (s, 24H, $OCH_3/-CH_{eq}H-$), 2.69 (bs, 12H, H_a). ESI-MS (+ve): $\{[Pd(en)]_3(Laz\text{-}OMe)_2\}^{6+}$ m/z 428.1710, calcd m/z 428.4311.

{[Pd(en)]$_3$(L_{az}-OEt)$_2$}·6(NO_3) ***(C2)***. ^{1}H NMR (500 MHz, d_6-DMSO): δ 9.62 (m, 6H, H_e), 9.15 (m, 6H, H_b), 8.51 (bs, 6H, H_d), 8.37 (t, 12H, J = 8.3 Hz, H_g), 8.10 (t, 12H, J = 8.3 Hz, H_f), 7.94 (t, 6H, J = 8.1 Hz, H_c), 7.56 (bs, 6H, H_i), 7.34 (bs, 6H, H_h), 5.67 (bs, 12H, NH), 4.87 (bs, 6H, $-CH_{ax}H-$), 4.04 (bs, 12H, OCH_2CH_3), 3.71 (bs, 6H, $-CH_{eq}H-$), 2.70 (bs, 12H, H_a), 1.16 (m, 18H, OCH_2CH_3).

{[Pd(en)]$_3$(L_{az}-OPr)$_2$}·6(NO_3) ***(C3)***. ^{1}H NMR (500 MHz, d_6-DMSO): δ 9.60 (m, 6H, H_e), 9.16 (m, 6H, H_b), 8.50 (bs, 6H, H_d), 8.35 (t, 12H, J = 8.6 Hz, H_g), 8.11 (t, 12H, J = 8.2 Hz, H_f), 7.95 (t, 6H, J = 8.0 Hz, H_c), 7.56 (bs, 6H, H_i), 7.35 (bs, 6H, H_h), 5.67 (bs, 12H, NH), 4.90 (bs, 6H, $-CH_{ax}H-$), 3.95 (bs, 12H, $OCH_2CH_2CH_3$), 3.72 (bs, 6H, $-CH_{eq}H-$), 2.70 (bs, 12H, H_a), 1.53 (bs, 12H, $OCH_2CH_2CH_3$), 0.79 (m, 18H, $OCH_2CH_2CH_3$).

Host–Guest Studies. All ^{1}H NMR titrations were performed at 300 K using the following procedure, given in detail for **C1** and SOS. A stock solution of **C1** was prepared in d_6-DMSO (3.85 mM, 2 mL); 0.55 mL of the stock was transferred to an NMR tube, and an initial ^{1}H NMR spectrum was acquired. SOS (19.7 mg, 84.8 μmol) was dissolved in 1 mL of the stock solution of **C1**. Aliquots of the solution containing SOS were added to the NMR tube incrementally such that the H:G ratio varied between 1:0.1 and 1:10. At each interval, the NMR tube was mixed with a vortex mixer and equilibrated for 5 min before the ^{1}H NMR spectrum was recorded. Binding isotherms were plotted using HypNMR2008.[44]

Crystallography. Single-crystal X-ray diffraction data were collected at 100 K using synchrotron radiation (λ = 0.6889 Å) at station I19 of the Diamond Light Source. Structures were determined using SHELXT[51] and refined by full-matrix least squares on F^2 with SHELXL[52] via the Olex2[53] and X-Seed[54] interfaces. All non-hydrogen atoms were refined anisotropically, and hydrogen atoms included at calculated positions. Both structures contained void space in the lattice with diffuse electron density that could not be meaningfully refined as solvent positions; hence, a solvent mask was applied through Olex2. For L_{az}-OPr·$CHCl_3$, the bond length of one azo group was restrained.

■ ASSOCIATED CONTENT

Supporting Information

The Supporting Information is available free of charge at https://pubs.acs.org/doi/10.1021/acs.inorgchem.1c01297.

Full reaction schemes, NMR spectra, UV–vis spectra, mass spectra, fitting of NMR binding data, crystallographic tables, and additional crystal structures (PDF)

Accession Codes

CCDC 2079170–2079171 contain the supplementary crystallographic data for this paper. These data can be obtained free of charge via www.ccdc.cam.ac.uk/data_request/cif, or by emailing data_request@ccdc.cam.ac.uk, or by contacting The Cambridge Crystallographic Data Centre, 12 Union Road, Cambridge CB2 1EZ, UK; fax: +44 1223 336033.

■ AUTHOR INFORMATION

Corresponding Author

Michaele J. Hardie − *School of Chemistry, University of Leeds, Leeds LS2 9JT, U.K.*; orcid.org/0000-0001-6586-7981; Email: m.j.hardie@leeds.ac.uk

Authors

Edward Britton − *School of Chemistry, University of Leeds, Leeds LS2 9JT, U.K.*

Richard J. Ansell − *School of Chemistry, University of Leeds, Leeds LS2 9JT, U.K.*

Mark J. Howard − *School of Chemistry, University of Leeds, Leeds LS2 9JT, U.K.*

Complete contact information is available at: https://pubs.acs.org/10.1021/acs.inorgchem.1c01297

Notes

The authors declare no competing financial interest.

Data accessibility: data supporting this study are available at https://doi.org/10.5518/1025.

■ ACKNOWLEDGMENTS

The authors thank the EPSRC for a studentship (1799710) for E.B. This work was carried out with support of the Diamond Light Source (MT-20570). The authors acknowledge the support of the Henry Royce Institute for E.B. through the Royce PhD Equipment Access Scheme enabling access to soft ionization and imaging mass spectrometry facilities at Royce@Liverpool (EPSRC Grant EP/R00661X/1). The authors thank Dwayne Heard's research group for access and assistance with the YAG laser, Christopher M. Pask for assistance with collection of X-ray data, and Matthew Snelgrove for assistance.

■ REFERENCES

(1) Selected recent reviews: (a) Pullen, S.; Clever, G. H. Mixed-Ligand Metal-Organic Frameworks and Heteroleptic Coordination Cages as Multifunctional Scaffolds-A Comparison. *Acc. Chem. Res.* **2018**, *51*, 3052–3064. (b) Vasdev, R. A. S.; Preston, D.; Crowley, J. D. Multicavity metallosupramolecular architectures. *Chem. - Asian J.* **2017**, *12*, 2513–2523. (c) Chen, L.-J.; Yang, H.-B.; Shionoya, M. Chiral metallosupramolecular architectures. *Chem. Soc. Rev.* **2017**, *46*, 2555–2576. (d) Ward, M. D.; Hunter, C. A.; Williams, N. H. Guest Binding and Catalysis in the Cavity of a Cubic Coordination Cage. *Chem. Lett.* **2017**, *46*, 2–9. (e) Chen, L.; Chen, Q.; Wu, M.; Jiang, F.; Hong, M. Controllable coordination-driven self-assembly: from discrete metallocages to infinite cage-based frameworks. *Acc. Chem. Res.* **2015**, *48*, 201–210. (f) Zarra, S.; Wood, D. M.; Roberts, D. A.; Nitschke, J. R. Molecular containers in complex chemical systems. *Chem. Soc. Rev.* **2015**, *44*, 419–432. (g) Chakrabarty, R.; Mukherjee, P. S.; Stang, P. J. Supramolecular Coordination: Self-Assembly of Finite Two- and Three-Dimensional Ensembles. *Chem. Rev.* **2011**, *111*, 6810–6918. (h) Harris, K.; Fujita, D.; Fujita, M. Giant hollow

M_nL_{2n} spherical complexes: structure, functionalisation and applications. *Chem. Commun.* **2013**, *49*, 6703−6712.
(2) Review: McConnell, A. J.; Wood, C. S.; Neelakandan, P. P.; Nitschke, J. R. Stimuli-Responsive Metal−Ligand Assemblies. *Chem. Rev.* **2015**, *115*, 7729−7793.
(3) (a) Murase, T.; Sato, S.; Fujita, M. Switching the interior hydrophobicity of a self-assembled spherical complex through the photoisomerization of confined azobenzene chromophores. *Angew. Chem., Int. Ed.* **2007**, *46*, 5133−5136. (b) Park, J.; Sun, L.-B.; Chen, Y.-P.; Perry, Z.; Zhou, H.-C. Azobenzene-Functionalized Metal−Organic Polyhedra for the Optically Responsive Capture and Release of Guest Molecules. *Angew. Chem., Int. Ed.* **2014**, *53*, 5842.
(4) Fu, S.; Luo, Q.; Zang, M.; Tian, J.; Zhang, Z.; Zeng, M.; Ji, Y.; Xu, J.; Liu, J. Light-triggered reversible disassembly of stimuli-responsive coordination metallosupramolecular Pd2L4 cages mediated by azobenzene-containing ligands. *Mater. Chem. Front.* **2019**, *3*, 1238−1243.
(5) (a) Li, R.-J.; Tessarolo, J.; Lee, H.; Clever, G. H. Multi-stimuli Control over Assembly and Guest Binding in Metallosupramolecular Hosts Based on Dithienylethene Photoswitches. *J. Am. Chem. Soc.* **2021**, *143*, 3865−3873. (b) Li, R.-J.; Holstein, J. J.; Hiller, W. G.; Andréasson; Clever, G. H. Mechanistic Interplay between Light Switching and Guest Binding in Photochromic [Pd_2Dithienylethene$_4$] Coordination Cages. *J. Am. Chem. Soc.* **2019**, *141*, 2097−2103. (c) Li, R.-J.; Han, M.; Tessarolo, J.; Holstein, J. J.; Lübben; Dittrich, B.; Volkmann, C.; Finze, M.; Jenne, C.; Clever, G. H. Successive Photoswitching and Derivatization Effects in Photochromic Dithienylethene-Based Coordination Cages. *ChemPhotoChem.* **2019**, *3*, 378−383. (d) Han, M.; Michel, R.; He, B.; Chen, Y.-S.; Stalke, D.; John, M.; Clever, G. H. Light-Triggered Guest Uptake and Release by a Photochromic Coordination Cage. *Angew. Chem., Int. Ed.* **2013**, *52*, 1319−1323.
(6) Han, M.; Luo, Y.; Damaschke, B.; Gómez, L.; Ribas, X.; Jose, A.; Peretzki, P.; Seibt, M.; Clever, G. H. Light-Controlled Interconversion between a Self-Assembled Triangle and a Rhombicuboctahedral Sphere. *Angew. Chem., Int. Ed.* **2016**, *55*, 445−449.
(7) Gu, Y.; Alt, E. A.; Wang, H.; Li, X.; Willard, A. P.; Johnson, J. A. Photoswitching topology in polymer networks with metal−organic cages as crosslinks. *Nature* **2018**, *560*, 65−69.
(8) Stuckhardt, C.; Roke, D.; Danowski, W.; Otten, E.; Wezenberg, S. J.; Feringa, B. L. A chiral self-sorting photoresponsive coordination cage based on overcrowded alkenes. *Beilstein J. Org. Chem.* **2019**, *15*, 2767−2773.
(9) Lee, J.; Brewster, J. T.; Song, B.; Lynch, V. M.; Hwang, I.; Li, X.; Sessler, J. L. Uranyl dication mediated photoswitching of a calix[4]pyrrole-based metal coordination cage. *Chem. Commun.* **2018**, *54*, 9422−9425.
(10) Oldknow, S.; Rota Martir, D.; Pritchard, V. E.; Blitz, M. A.; Fishwick, C. W. G.; Zysman-Colman, E.; Hardie, M. J. Structure-switching M_3L_2 Ir(III) coordination cages with photo-isomerizing azo-aromatic groups. *Chem. Sci.* **2018**, *9*, 8150−8159.
(11) Review: Wezenberg, S. J. Light-switchable metal-organic cages. *Chem. Lett.* **2020**, *49*, 609−615.
(12) (a) Hardie, M. J. Cyclotriveratrylene and cryptophanes. In *Supramolecular Chemistry: From Molecules to Nanomaterials*; Gale, P. A., Steed, J. W., Eds.; John Wiley & Sons, 2012; Vol. 3, pp 895−916. (b) Collet, A. Cyclotriveratrylenes and cryptophanes. *Tetrahedron* **1987**, *43*, 5725−5759.
(13) Reviews: (a) Hardie, M. J. Self-assembled cages and capsules using cyclotriveratrylene-type scaffolds. *Chem. Lett.* **2016**, *45*, 1336−1346. (b) Henkelis, J. J.; Hardie, M. J. Controlling the assembly of cyclotriveratrylene-derived coordination cages. *Chem. Commun.* **2015**, *51*, 11929−11943.
(14) Zhong, Z.; Ikeda, A.; Shinkai, S.; Sakamoto, S.; Yamaguchi, K. Creation of Novel Chiral Cryptophanes by a Self-Assembling Method Utilizing a Pyridyl−Pd(II) Interaction. *Org. Lett.* **2001**, *3*, 1085−1087.
(15) Schaly, A.; Rousselin, Y.; Chambron, J.-C.; Aubert, E.; Espinosa, E. The Stereoselective Self-Assembly of Chiral Metallo-Organic Cryptophanes. *Eur. J. Inorg. Chem.* **2016**, *2016*, 832−843.
(16) Schaly, A.; Meyer, M.; Chambron, J.-C.; Jean, M.; Vanthuyne, N.; Aubert, E.; Espinosa, E.; Zorn, N.; Leize-Wagner, E. The chemo- and stereoselective formation of pallado- and platinocryptophanes. *Eur. J. Inorg. Chem.* **2019**, *2019*, 2691−2706.
(17) Cookson, N. J.; Fowler, J. M.; Martin, D. P.; Fisher, J.; Henkelis, J. J.; Ronson, T. K.; Thorp-Greenwood, F. L.; Willans, C. E.; Hardie, M. J. Metallo-cryptophane cages from *cis*-linked and *trans*-linked strategies. *Supramol. Chem.* **2018**, *30*, 255−266.
(18) Fujita, M.; Umemoto, K.; Yoshizawa, M.; Fujita, N.; Kusukawa, T.; Biradha, K. Molecular panelling via coordination. *Chem. Commun.* **2001**, 509−518.
(19) Henkelis, J. J.; Carruthers, C. J.; Chambers, S. E.; Clowes, R.; Cooper, A. I.; Fisher, J.; Hardie, M. J. Metallo-cryptophanes decorated with bis-N-heterocyclic carbene ligands: self-assembly and guest uptake into a non-porous crystalline lattice. *J. Am. Chem. Soc.* **2014**, *136*, 14393−14396.
(20) Chand, D. K.; Manivannan, R.; Sahoo, H. S.; Jeyakumar, K. Self-assembly by ligand-exchange reactions. *Eur. J. Inorg. Chem.* **2005**, *2005*, 3346−3352.
(21) Pritchard, V. E.; Rota Martir, D.; Oldknow, S.; Kai, S.; Hiraoka, S.; Cookson, N. J.; Zysman-Colman, E.; Hardie, M. J. Homochiral self-sorted and emissive Ir(III) metallo-cryptophanes. *Chem. - Eur. J.* **2017**, *23*, 6290−6294.
(22) Bandara, H. M. D.; Burdette, S. C. Photoisomerization in different classes of azobenzene. *Chem. Soc. Rev.* **2012**, *41*, 1809−1825.
(23) Sun, S.-S.; Anspach, J. A.; Lees, A. J. Self-Assembly of Transition-Metal-Based Macrocycles Linked by Photoisomerizable Ligands: Examples of Photoinduced Conversion of Tetranuclear−Dinuclear Squares. *Inorg. Chem.* **2002**, *41*, 1862−1869.
(24) Henkelis, J. J.; Fisher, J.; Warriner, S. L.; Hardie, M. J. Solvent-dependent chiral self-sorting, and stoichiometric speciation control of metallo-supramolecular cages. *Chem. - Eur. J.* **2014**, *20*, 4117−4125.
(25) Lincoln, S. F. Mechanistic Studies of Metal Aqua Ions: A Semi-Historical Perspective. *Helv. Chim. Acta* **2005**, *88*, 523−545.
(26) Canceill, J.; Collet, A.; Gabard, J.; Gottarelli, G.; Spada, G. P. Exciton approach to the optical activity of C3-cyclotriveratrylene derivatives. *J. Am. Chem. Soc.* **1985**, *107*, 1299−1308.
(27) Illa, G. T.; Hazra, S.; Satha, P.; Purohit, C. S. Hydrogen-bonded molecular capsules: probing the role of water molecules in capsule formation in modified cyclotricatechylene. *CrystEngComm* **2017**, *19*, 4759−4765.
(28) Reviews: (a) Lu, Y.; Zhang, H.-N.; Jin, G.-X. Molecular Borromean Rings Based on Half-Sandwich Organometallic Rectangles. *Acc. Chem. Res.* **2018**, *51*, 2148−2158. (b) Pan, M.; Su, C.-Y. Coordination assembly of Borromean structures. *CrystEngComm* **2014**, *16*, 7847−7859. (c) Cantrill, S. J.; Chichak, K. S.; Peters, A. J.; Stoddart, J. F. Nanoscale Borromean Rings. *Acc. Chem. Res.* **2005**, *38*, 1−9.
(29) Thorp-Greenwood, F. L.; Kulak, A. N.; Hardie, M. J. An infinite chainmail of M_6L_6 metallacycles featuring multiple Borromean links. *Nat. Chem.* **2015**, *7*, 526−531.
(30) For example: (a) Huan, D.-M.; Liu, Y.-G.; Yu, B.; Cui, G.-H. 1D ladder-like chain and 3-fold Borromean entanglement of silver(I) coordination polymers with different metal salts. *Inorg. Chem. Commun.* **2016**, *67*, 17−21. (b) Carlucci, L.; Ciani, G.; Proserpio, D. M. Borromean links and other non-conventional links in 'polycatenated' coordination polymers: re-examination of some puzzling networks. *CrystEngComm* **2003**, *5*, 269−279.
(31) For example: Men, Y.-B.; Sun, J.; Huang, Z.-T.; Zheng, Q.-Y. Rational construction of 2D and 3D borromean arrayed organic crystals by hydrogen-bond-directed self-assembly. *Angew. Chem., Int. Ed.* **2009**, *48*, 2873−2876.
(32) Men, Y.-B.; Sun, J.; Huang, Z.-T.; Zheng, Q.-Y. Design and construction of an organic crystal with a novel interpenetrated n-Borromean linked topology. *Chem. Commun.* **2010**, *46*, 6299−6301.
(33) Kumar, V.; Pilati, T.; Terraneo, G.; Meyer, F.; Metrangolo, P.; Resnati, G. Halogen bonded Borromean networks by design: topology invariance and metric tuning in a library of multi-component systems. *Chem. Sci.* **2017**, *8*, 1801−1810.

https://doi.org/10.1021/acs.inorgchem.1c01297
Inorg. Chem. 2021, 60, 12912−12923

(34) Dobrzanska, L.; Raubenheimer, H. G.; Barbour, L. J. Borromean sheets assembled by self-supporting argentophilic interactions. *Chem. Commun.* **2005**, 5050−5052.
(35) Shi, X.; Wang, W.; Hou, H.; Fan, Y. A Hydroscopic Self-Catenated Net Formed by Borromean Layers Interlocked by Ferrocenyl Bridging Ligands. *Eur. J. Inorg. Chem.* **2010**, *2010*, 3652−3657.
(36) Pfeil, A.; Lehn, J.-M. Helicate self-organisation: positive cooperativity in the self-assembly of double-helical metal complexes. *J. Chem. Soc., Chem. Commun.* **1992**, 838−840.
(37) As for the $\{[Ir(C\wedge N)_2]_3(Laz)_2\}^{3+}$ cages,[8] a Nd:YAG laser was used as irradiation with a 30 W 365 nm lamp did not result in any switching behavior (see Figure S28 for such experiments with **C2**).
(38) Reviews: (a) Kalenius, E.; Groessl, M.; Rissanen, K. Ion mobility-mass spectrometry of supramolecular complexes and assemblies. *Nat. Rev. Chem.* **2019**, *3*, 4−14. (b) Brocker, E. R.; Anderson, S. E.; Northrop, B. H.; Stang, P. J.; Bowers, M. T. Structures of Metallosupramolecular Coordination Assemblies Can Be Obtained by Ion Mobility Spectrometry−Mass Spectrometry. *J. Am. Chem. Soc.* **2010**, *132*, 13486−13494.
(39) For example: Steed, J. W.; Junk, P. C.; Atwood, J. L.; Barnes, M. J.; Raston, C. L.; Burkhalter, R. S. Ball and Socket Nanostructures: New Supramolecular Chemistry Based on Cyclotriveratrylene. *J. Am. Chem. Soc.* **1994**, *116*, 10346−10347.
(40) Cookson, N. J.; Henkelis, J. J.; Ansell, R. J.; Fishwick, C. W. G.; Hardie, M. J.; Fisher, J. Encapsulation of sodium alkyl sulphates by the cyclotriveratrylene-based $[Pd_6L_8]^{12+}$ stella octangula cage. *Dalton Trans.* **2014**, *43*, 5657−5661.
(41) Lee, H.; Kim, D.; Oh, H.; Jung, O.-S. Molecular balloon, Pd_6L_8 cages: recognition of alkyl sulfate surfactants. *Chem. Commun.* **2020**, *56*, 2841−2844.
(42) Cai, L.; Gochin, M.; Liu, K. A facile surfactant critical micelle concentration determination. *Chem. Commun.* **2011**, *47*, 5527−5529.
(43) Note that the critical micelle concentrations are anticipated to be larger in DMSO solutions: Markarian, S. A.; Harutyunyan, L. R.; Harutyunyan, R. S. The Properties of Mixtures of Sodium Dodecylsulfate and Diethylsulfoxide in Water. *J. Solution Chem.* **2005**, *34*, 361−368.
(44) Frassineti, C.; Ghelli, S.; Gans, P.; Sabatini, A.; Moruzzi, M. S.; Vacca, A. Nuclear Magnetic Resonance as a Tool for Determining Protonation Constants of Natural Polyprotic Bases in Solution. *Anal. Biochem.* **1995**, *231*, 374−382.
(45) Yu, J.-S.; Wu, F.-G.; Zhou, Y.; Zheng, Y.-Z.; Yu, Z.-W. Selective recognition induced nanostructures in a cucurbit[7]uril-based host−guest system: micelles, nanorods and nanosheets. *Phys. Chem. Chem. Phys.* **2012**, *14*, 8506−8510.
(46) Mecozzi, S.; Rebek, J., Jr. The 55% Solution: A Formula for Molecular Recognition in the Liquid State. *Chem. - Eur. J.* **1998**, *4*, 1016−1022.
(47) Cao, X.; Meng, L.; Li, Z.; Mao, Y.; Lan, H.; Chen, L.; Fan, Y.; Yi, T. Large Red-Shifted Fluorescent Emission via Intermolecular $\pi-\pi$ Stacking in 4-Ethynyl-1,8-naphthalimide-Based Supramolecular Assemblies. *Langmuir* **2014**, *30*, 11753−11760.
(48) Williamson, M. P. Using chemical shift perturbation to characterize ligand binding. *Prog. Nucl. Magn. Reson. Spectrosc.* **2013**, *73*, 1−16.
(49) Ronson, T. K.; Meng, W.; Nitschke, J. R. Design Principles for the Optimization of Guest Binding in Aromatic-Paneled $Fe^{II}_4L_6$ Cages. *J. Am. Chem. Soc.* **2017**, *139*, 9698−9707.
(50) Brotin, T.; Roy, V.; Dutasta, J.-P. Improved Synthesis of Functional CTVs and Cryptophanes Using $Sc(OTf)_3$ as Catalyst. *J. Org. Chem.* **2005**, *70*, 6187−6195.
(51) Sheldrick, G. M. SHELXT − Integrated space-group and crystal structure determination. *Acta Crystallogr., Sect. A: Found. Adv.* **2015**, *71*, 3−8.
(52) Sheldrick, G. M. A short history of SHELX. *Acta Crystallogr., Sect. A: Found. Crystallogr.* **2008**, *A64*, 112−122.
(53) Dolomanov, O. V.; Bourhis, L. J.; Gildea, R. J.; Howard, J. A. K.; Puschmann, H. OLEX2: A complete structure solution, refinement and analysis program. *J. Appl. Crystallogr.* **2009**, *42*, 339−341.
(54) Barbour, L. J. X-Seed − A software tool for supramolecular crystallography. *J. Supramol. Chem.* **2001**, *1*, 189−191.

https://doi.org/10.1021/acs.inorgchem.1c01297
Inorg. Chem. 2021, 60, 12912−12923